Correlation Between SUV_{max} and CT Radiomic Analysis Using Lymph Node Density in PET/CT-Based Lymph Node Staging

Frederik L. Giesel[1,2], Florian Schneider[1], Clemens Kratochwil[1], Daniel Rath[1], Jan Moltz[3], Tim Holland-Letz[4], Hans-Ulrich Kauczor[5,6], Lawrence H. Schwartz[7], Uwe Haberkorn[1,2,6], and Paul Flechsig[1,5,6]

[1]Department of Nuclear Medicine, University Hospital Heidelberg, Heidelberg, Germany; [2]Clinical Cooperation Unit, Department of Nuclear Medicine, DKFZ, Heidelberg, Germany; [3]Fraunhofer Institute for Medical Image Computing, Bremen, Germany; [4]Department of Biostatistics, German Cancer Research Center, Heidelberg, Germany; [5]Department of Diagnostic and Interventional Radiology, University Hospital Heidelberg, Heidelberg, Germany; [6]Translational Lung Research Center Heidelberg, Heidelberg, Germany; and [7]Department of Radiology, New York–Presbyterian/Columbia University Medical Centre, New York, New York

In patients with lung cancer (LC), malignant melanoma (MM), gastroenteropancreatic neuroendocrine tumors (GEP NETs), and prostate cancer (PCA), lymph node (LN) staging is often performed by ^{18}F-FDG PET/CT (LC and MM), ^{68}Ga-DOTATOC PET/CT (GEP NET), and ^{68}Ga-labeled prostate-specific membrane antigen PET/CT (PCA) but is sometimes not accurate because of indeterminate PET findings. To better evaluate malignant LN infiltration, additional surrogate parameters, especially in cases with indeterminate PET findings, would be helpful. The purpose of this study was to evaluate whether SUV_{max} in the PET examination might correlate with semiautomated density measurements of LNs in the CT component of the PET/CT examination. **Methods:** After approval by the institutional review board, 1,022 LNs in the PET/CT examinations of 148 patients were retrospectively analyzed (LC: 327 LNs of 40 patients; MM: 224 LNs of 33 patients; GEP NET: 217 LNs of 35 patients; and PCA: 254 LNs of 40 patients). PET/CT was performed before surgery, biopsy, chemotherapy, or internal or external radiation therapy, according to the clinical schedule; patients with prior chemotherapy or radiation therapy were excluded. SUV_{max} analyses were based on uptake 60 min after tracer injection, and volumetric CT histogram analyses were based on the unenhanced CT images of the PET/CT scan. **Results:** PET findings were considered positive or negative on the basis of SUV_{max} in the LN compared with that in the blood pool; histologic confirmation was not available. Of the 1,022 LNs, 331 were PET-positive (3 times the SUV_{max} of the blood pool), 86 were PET-indeterminate (1–3 times the SUV_{max} of the blood pool), and 605 were PET-negative (less than the SUV_{max} of the blood pool). PET-positive LNs had significantly higher CT densities than PET-negative LNs, irrespective of the type of cancer. **Conclusion:** CT density measurements of LNs in patients with LC, MM, GEP NET, and PCA correlated with ^{18}F-FDG uptake, ^{68}Ga-DOTATOC uptake, and ^{68}Ga-PSMA uptake, respectively, and might therefore serve as an additional surrogate parameter for differentiating between malignant and benign LNs. The use of a 7.5–Hounsfield unit CT density threshold to differentiate between malignant and benign LN infiltration and 20 Hounsfield units to exclude benign LN processes might be possible in clinical routine and would be especially helpful for PET-indeterminate LNs.

Key Words: N staging; FDG PET/CT; DOTATOC PET/CT; PSMA PET/CT; radiomics

J Nucl Med 2017; 58:282–287
DOI: 10.2967/jnumed.116.179648

One of the most widespread and reliable noninvasive staging tools for cancer is PET/CT—namely, ^{18}F-FDG PET/CT for lung cancer (LC (*1,2*)) and malignant melanoma (MM (*1,3*)), ^{68}Ga-labeled prostate-specific membrane antigen (PSMA) PET/CT for prostate cancer (PCA (*4*)), and ^{68}Ga-DOTATOC PET/CT for gastroenteropancreatic neuroendocrine tumors (GEP NETs (*5*)). An exact evaluation of lymph node (LN) status before therapy is crucial to therapy planning. False-positive PET findings are not uncommon with ^{18}F-FDG PET/CT, because the scan can mistakenly pick up on inflammation due to infectious etiologies, such as in the lung or the head and neck (*3,6*). Therefore, invasive LN staging is mandated by various guidelines to verify PET-positive LNs, especially when curative therapy is intended (*7*). To further develop imaging biomarkers and to capture intratumoral heterogeneity noninvasively, we applied techniques used in the rapidly evolving field of radiomics (*8*).

To assess for possible correlations between the functional PET and morphologic CT components of PET/CT, metric and functional parameters including volumetric CT histogram analysis, CT density, and SUV_{max} were evaluated in the LNs of patients with LC, MM, GEP NET, and PCA. For LC patients, increased CT density in metastatic LNs has been found by two studies, with cohorts of 45 (*6*) and 72 (*9*) patients. For MM patients, GEP NET, and PCA, no data correlating histologic LN status, SUV_{max}, and CT density are, to our knowledge, currently available.

We hypothesized that in LN metastases from these types of cancer, positive correlations between tracer accumulation, as a functional measure of malignant LN infiltration, and CT densities, as a possible surrogate metric parameter for LN infiltration, might be evident. Therefore, CT density was defined as the primary endpoint, and short-axis diameter (SAD) and SUV_{max} were regarded as secondary endpoints.

Received Jun. 9, 2016; revision accepted Aug. 10, 2016.
For correspondence or reprints contact: Paul Flechsig, Department of Nuclear Medicine, University Hospital Heidelberg, INF 400, 69120 Heidelberg, Germany.
E-mail: paul.flechsig@med.uni-heidelberg.de
Published online Sep. 22, 2016.

MATERIALS AND METHODS

Study Design

The study took place at a single center, was approved by the institutional review board, and was conducted according to the guidelines of the board and good clinical practice, adhering to the ethical principles originating in the Declaration of Helsinki. For this retrospective analysis, the institutional review board waived the requirement for informed consent.

Patients

In total, 1,022 LNs in 148 patients (86 male and 62 female; median age, 62 y) were examined (LC: 327 LNs of 40 patients; MM: 224 LNs of 33 patients; GEP NET: 217 LNs of 35 patients; and PCA: 254 LNs of 40 patients). All PET/CT examinations were performed for staging and therapeutic planning according to the clinical schedule before surgical resection, chemotherapy, or radiation therapy. Any patients who had undergone neoadjuvant radiation or chemotherapy before the PET/CT examination were excluded.

Radionuclide Administration

^{18}F-FDG PET/CT imaging began 60 ± 5 min after intravenous injection of 4 MBq of ^{18}F-FDG per kilogram of body weight (following a fast of ≥8 h, and with a blood glucose level of <150 mg/dL). ^{68}Ga-DOTATOC PET/CT imaging began 60 ± 5 min after intravenous injection of 80–200 MBq of ^{68}Ga-DOTATOC. ^{68}Ga-PSMA PET/CT imaging began 60 ± 5 min after injection of 150–250 MBq of ^{68}Ga-PSMA.

PET/CT Acquisition and Image Reconstruction

A Biograph 6 PET/CT scanner (Siemens Medical Solutions) was used, with a slice thickness of 5.0 mm, a reconstruction increment of 2.5 mm, and a standard B30 soft-tissue reconstruction kernel. Static emission scans (8 bed positions at 4 min each) were acquired from the vertex to the proximal legs with correction for dead time, scatter, and decay. For attenuation correction, unenhanced low-dose CT was used (*10*).

Emission images were iteratively reconstructed using ordered-subset expectation maximization (4 iterations, 8 subsets, and gaussian filtering), resulting in an in-plane spatial resolution of 5 mm in full width at half maximum (*10,11*).

SUV_{max} Analysis

^{18}F-FDG uptake, ^{68}Ga-DOTATOC uptake, and ^{68}Ga-PSMA uptake were evaluated using SUV_{max}. In our department, the clinical standard for evaluating LNs on ^{18}F-FDG PET/CT is to classify them as PET-positive (PET+) when the SUV_{max} is more than 3 times that of the blood pool, PET-indeterminate (PET+/−) when 1–3 times that of the blood pool, and PET-negative (PET−) when less than or equal to that of the blood pool, irrespective of tumor type and tracer.

CT Radiomic Analysis

Morphologic LN assessment and volumetric CT histogram analysis were performed by a radiologist with 5 y of experience in oncologic imaging, without access to the clinical information. Volumetric LN analysis was performed semiautomatically using software developed at the Fraunhofer Institute for Medical Image Computing (*12*).

The CT density and SAD analyses were performed on the unenhanced native CT scans of the PET/CT examinations using dedicated software for semiautomated LN segmentation (*6*). The analyses were initiated by providing a seed point in the investigated LN. The segmentation software automatically generated thresholds within an estimated region of interest; this semiautomated segmentation process alone had a high level of reproducibility—at least 90% (*6*). In a next step, the software automatically extracted spatial parameters and analyzed the histograms (*6*). The results of the semiautomated LN evaluation were validated by the conducting physician, who visually went through all 3 dimensions of each assessed LN using the integrated 3-dimensional viewer for multiplanar reconstruction (*6*). If necessary, the semiautomated segmentation was corrected manually in all 3 dimensions.

Statistical Analysis

Statistical analysis was performed using SigmaPlot (Systat Software GmbH). Median CT density, SAD, and SUV_{max} with 95% confidence interval were calculated and presented as box-and-whisker plots. Differences were considered significant at a P value of less than 0.05 on 2-sided paired-sample t testing for SAD and CT density and on 2-sided Wilcoxon signed rank testing for SUV_{max}. The diagnostic accuracy of all 4 variables was analyzed using receiver-operating-characteristic curves.

RESULTS

PET Findings

Among the various tumor types, the number of PET+, PET+/−, and PET− LNs was distributed as shown in Table 1 and Figure 1. Except for the GEP NET patients, for whom SUV_{max} was either below the level of the mediastinal blood pool or more than triple the blood-pool level, PET+, PET+/−, and PET− LNs were found for all tumor types.

Metric and Functional LN Analysis

For semiautomated LN analysis, less than 1 min of additional time was needed to evaluate each LN, including semiautomated size and CT density measurements.

LC Patients. For LC patients, CT density was significantly higher in PET+ LNs (31.3 Hounsfield units [HU]) than in PET− LNs (−12.6 HU; $P < 0.01$) (Table 1; Fig. 2A), which correlated well with the corresponding LN histograms of averaged PET+, PET+/−, and PET− LNs (Fig. 2B). SAD was significantly higher in PET+ LNs (12.7 mm) than in PET+/− LNs (7.8 mm; $P < 0.01$) or PET− LNs (5.7 mm; $P < 0.01$) (Table 1; Fig. 2C).

MM Patients. For MM patients, CT density was significantly higher in PET+ LNs (27.9 HU) than in PET− LNs (−16.3 HU, $P < 0.01$) (Table 1; Fig. 3A), which correlated well with the corresponding LN histograms of averaged PET+, PET+/−, and PET− LNs (Fig. 3B). SAD was significantly higher in PET+ LNs (10 mm) than in PET+/− LNs (8.3 mm, $P < 0.05$) or PET− LNs (5 mm, $P < 0.01$) (Table 1; Fig. 3C).

GEP NET Patients. For GET NET patients, since there were no PET-indeterminate LNs, it was possible to correlate only PET+ and PET− LNs. CT density was significantly higher in PET+ LNs (33.7 HU) than in PET− LNs (−11.6 HU, $P < 0.01$) (Table 1; Fig. 4A). This was also evident in the corresponding LN histograms of averaged PET+ and PET− LNs (Fig. 4B). The SAD of PET+ LNs (9.7 mm) was significantly higher than that of PET− LNs (5.6 mm, $P < 0.01$) (Table 1; Fig. 4C).

PCA Patients. For PCA patients, CT density was significantly higher in PET+ LNs (19.2 HU) than in PET− LNs (−23.7 HU, $P < 0.01$) (Table 1; Fig. 5A). There was no significant difference in CT density between PET+LNs (19.2 HU) and PET+/− LNs (9.9 HU, $P = 0.06$) (Table 1); nevertheless, CT density tended to

TABLE 1
Correlation Between PET and CT Data

Tumor type	PET+	PET+/−	PET−	*P*		
				+ vs. +/−	+ vs. −	+/− vs. −
LC						
No. of LNs	75	48	204			
CT density (HU)	31.3 (−10.4/39.2)	27.6 (−17.2/69.8)	−12.57 (−56.3/17.9)	0.08	<0.01	<0.05
SAD (mm)	12.7 (4.1/32.1)	7.8 (3.1/17.3)	5.7 (1.9/14.2)	<0.01	<0.01	0.12
MM						
No. of LNs	79	27	118			
CT density (HU)	27.9 (−16.7/66.4)	19.1 (−15/55.7)	−16.3 (−69/21.2)	0.13	<0.01	<0.01
SAD (mm)	10 (4.1/35.8)	8.3 (3.1/20)	5 (2.1/8.1)	<0.05	<0.01	<0.01
GEP NET						
No. of LNs	77	0	140			
CT density (HU)	33.7 (−10.6/69.5)	—	−11.6 (−64/19.4)	—	<0.01	—
SAD (mm)	9.7 (3.1/36.8)	—	5.6 (2/12.3)	—	<0.01	—
PCA						
No. of LNs	100	11	143			
CT density (HU)	19.2 (−44.2/47.1)	9.9 (−10.6/42.9)	−23.7 (−68.8/27)	0.06	<0.01	<0.05
SAD (mm)	7.1 (3.1/22.7)	8.3 (5.5/12.6)	5.5 (1.9/9.9)	0.78	<0.01	0.21

Data in parentheses are minimum and maximum. Number of LNs is according to PET status. *P* values are for 2-sided *t* testing between subgroups.

be lower in PET+/− LNs than in PET+ LNs. CT density significantly differed between PET+/− and PET− LNs ($P < 0.01$) (Table 1). The corresponding LN histograms of averaged PET+, PET+/−, and PET− LNs are shown in Figure 5B. SAD was significantly higher in PET+ LNs (7.1 mm) than in PET− LNs (5.5 mm, $P < 0.01$), but there was no statistically significant difference in SAD between PET+ and PET+/− LNs ($P = 0.78$) (Table 1; Fig. 5C) or between PET+/− and PET− LNs ($P = 0.21$) (Table 1; Fig. 5C).

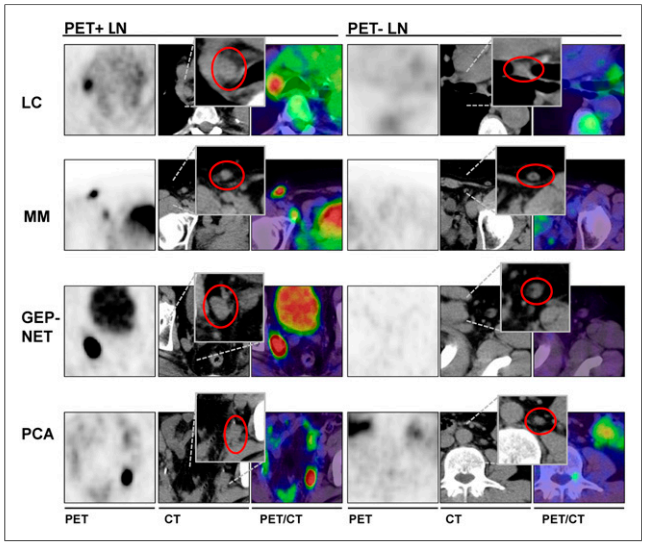

FIGURE 1. PET image, native CT image with magnified LN (circled) for CT density analysis, and PET/CT image in patients with LC, MM, GEP NET, and PCA.

CT Density–Based Cutoff

The CT density–based cutoff data are presented in Table 1.

In LC patients, 96% of PET+ LNs had a CT density of more than 7.5 HU, whereas 91% of PET− LNs had a CT density of less than 7.5 HU (Fig. 2A); the CT density of all PET− LNs was less than 20 HU. In MM patients, 91% of PET+ LNs had a CT density of more than 7.5 HU, whereas 90% of PET− LNs had a CT density of less than 7.5 HU (Fig. 3A); the CT density of 99% of PET− LNs was less than 20 HU. In GEP NET patients, 96% of PET+ LNs had a CT density of more than 7.5 HU, whereas 89% of PET− LNs had a CT density of less than 7.5 HU (Fig. 4A); the CT density of all PET− LNs was less than 20 HU. In PCA patients, 77% of PET+ LNs had a CT density of more than 7.5 HU, whereas 96% of PET− LNs had a CT density of less than 7.5 HU (Fig. 5A); the CT density of 99% of PET− LNs was less than 20 HU.

Regarding all LNs irrespective of tumor type, 89% of PET+ LNs had a CT density of more than 7.5 HU, whereas more than 92% of PET− LNs had a CT density of less than 7.5 HU (Fig. 6). More than 99% of PET− LNs had a CT density of less than 20 HU (Fig. 6). Nearly half the PET+/− LNs had a CT density of less than 20 HU (43%), and 83% had a CT density of more than 7.5 HU (Fig. 6).

Receiver-Operating-Characteristic Analyses

Higher areas under the receiver-operating-characteristic curve were calculated for CT density than for SAD for all tumor types, using PET positivity as the standard of reference. The areas under the curve for CT density versus SAD were 0.99 versus 0.93 for LC (Supplemental Fig. 1), 0.97 versus 0.89 for MM (Supplemental Fig. 2), 0.98 versus 0.85 for GEP NET (Supplemental Fig. 3), and 0.92 versus 0.7 for PCA (Supplemental Fig. 4). These data indicate a higher correlation between PET and CT density than between PET and SAD. (The supplemental figures are available at http://jnm.snmjournals.org.)

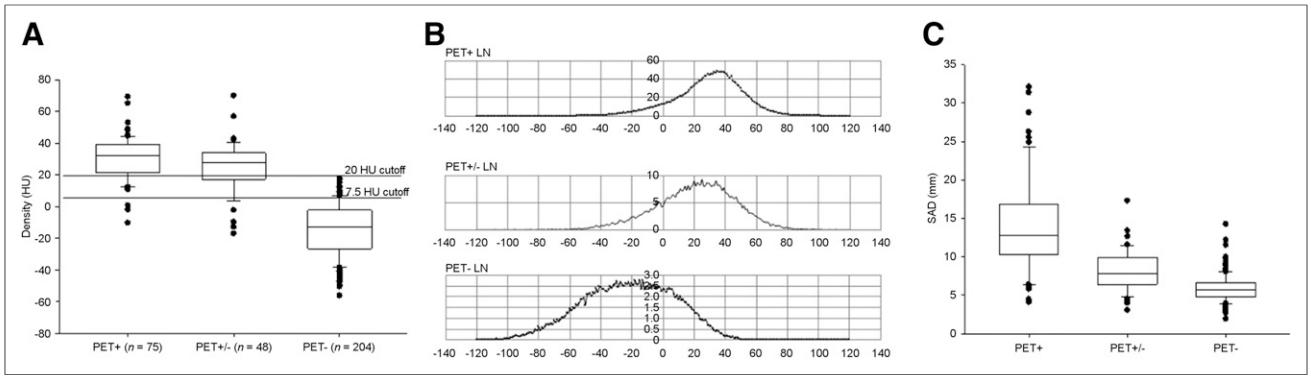

FIGURE 2. Statistical analysis of CT density in LC patients. (A) Box plots with median and 95% confidence interval for PET+, PET+/−, and PET− LNs. (B) Averaged histograms for PET+, PET+/−, and PET− LNs. (C) Box plots with median, 25%, and 75% quartiles for PET+, PET+/−, and PET− LNs. *P* values for statistical analysis among subgroups are presented in Table 1.

DISCUSSION

Using semiautomated CT histogram analysis, we found significantly higher CT densities in PET+ LNs than PET− LNs in patients with LC, MM, GEP NET, and PCA. In the ^{18}F-FDG PET/CT examinations of MM patients, we also found significantly higher densities in PET+ LNs than in PET+/− LNs. Regarding receiver-operating-characteristic analyses with PET positivity as the standard of reference, we found larger areas under the curve for CT density than for the metric parameter SAD, which is commonly used in RECIST (version 1.1). With the hypothesis that PET positivity is a measure for malignant LN infiltration in these types of tumor (which needs to be confirmed and validated in an independent cohort of patients), a possible cutoff of 7.5 HU might serve as an additional surrogate parameter for differentiating between malignant and benign LN involvement in patients with LC, MM, GEP NET, and PCA. In the cohort of 1,022 LNs, irrespective of tumor type, 89% of PET+ LNs had densities above the 7.5-HU cutoff, whereas 92% of PET− LNs had densities below the 7.5-HU cutoff. Thus, a possible cutoff of 7.5 HU might help to further discriminate between benign and malignant LN infiltration, which is of particular clinical relevance for PET+/− LNs, with 83% of such LNs having CT densities above the 7.5-HU cutoff.

Another cutoff, 20 HU, might help exclude benign LNs. More than 99% of benign LNs fell beneath this cutoff, indicating that LNs with CT densities of more than 20 HU are most likely to be malignant. This finding is of outstanding clinical interest because of the integral role of exact LN classification in diagnostic staging, therapy stratification, and postsurgical follow-up imaging.

The fact that PET positivity is a clinically valuable measure for malignant LN infiltration has been demonstrated by a study that found a sensitivity of 89%, specificity of 84%, and negative predictive value of 96% in LC patients (*13*). The value of PET/CT for staging and follow-up in MM patients was proven in several studies, which found a sensitivity of 96%, specificity of 92%, positive predictive value of 92%, and negative predictive value of 95% for neoplastic relapse, as summarized in a systematic review (*14*). Regarding patients with somatostatin receptor–positive GEP NETs, several studies demonstrated the excellent clinical use of ^{68}Ga-DOTATOC PET/CT for the detection of primary tumors, LN metastases, and distant metastases, as well as the potential of somatostatin receptor–based therapies (*15*). In PCA patients, a recently published study found a sensitivity of 86.9%, specificity of 93.1%, positive predictive value of 75.7%, and negative predictive value of 96.6% for LN staging on ^{68}Ga-PSMA PET/CT (*4*).

A possible CT density cutoff of 20 HU for LN staging in LC patients, with histopathologic correlation as the standard of reference, has been proposed by one group (*6*). Other groups have found strong correlations between CT density, SUV_{max} ratio, and malignant LN infiltration in patients with non–small cell lung cancer without mentioning a dedicated, CT density–based cutoff feasible for clinical routine (*9*). Recently published data from an animal study showed possible

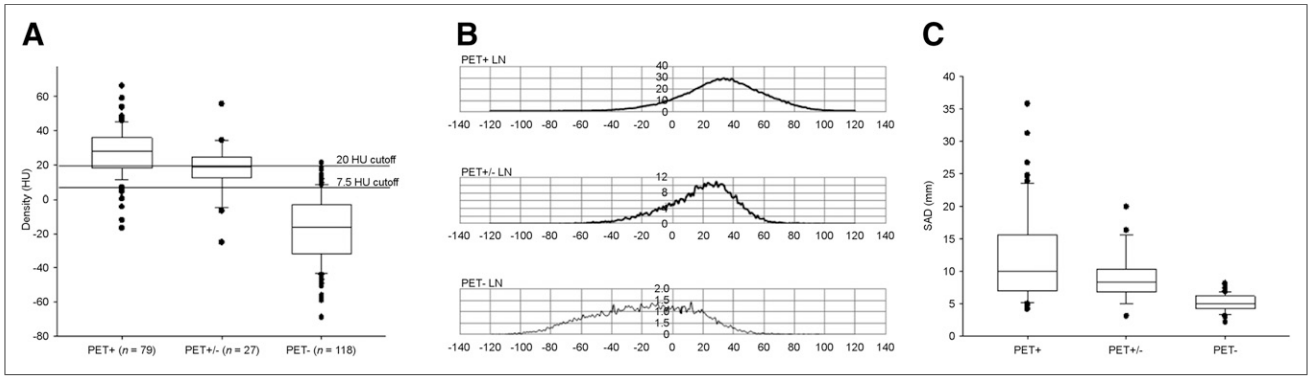

FIGURE 3. Statistical analysis of CT density in MM patients. (A) Box plots with median and 95% confidence interval for PET+, PET+/−, and PET− LNs. (B) Averaged histograms for PET+, PET+/−, and PET− LNs. (C) Box plots with median, 25%, and 75% quartiles for PET+, PET+/−, and PET− LNs. *P* values for statistical analysis among subgroups are presented in Table 1.

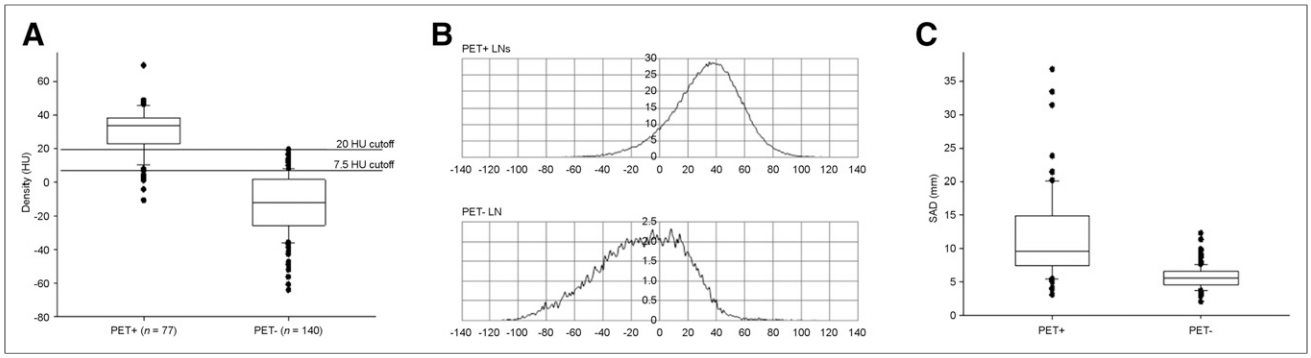

FIGURE 4. Statistical analysis of CT density in patients with GEP NET. (A) Box plots with median and 95% confidence interval for PET+, PET+/−, and PET− LNs. (B) Averaged histograms for PET+, PET+/−, and PET− LNs. (C) Box plots with median, 25%, and 75% quartiles for PET+, PET+/−, and PET− LNs. *P* values for statistical analysis among subgroups are presented in Table 1.

CT density–based cutoffs for differentiating between malignant and benign LNs without mentioning a possible cutoff that might be applied to humans (*16*).

In LC patients, ^{18}F-FDG PET/CT has shown high diagnostic accuracy in terms of LN staging (*13,17–22*), with the exception of very small LNs that need invasive intrathoracic LN sampling (*23*). In clinical routine, combined analysis of the metric parameter SAD (according to RECIST 1.1) and the functional parameter SUV_{max}, usually performed using ^{18}F-FDG PET/CT, allows for the most reliable noninvasive staging (*24–26*). According to McIvor et al., ^{18}F-FDG PET/CT helped detect unsuspected sites of MM in 17% of early-stage disease—a time when established guidelines usually recommend that ^{18}F-FDG PET/CT not be performed (*27*). According to Zattoni et al. (*28*), pretherapeutic ^{68}Ga-PSMA PET/CT helped find possible high-yield targets for salvage LN dissection in PCA patients, but the authors still stated the need for novel biomarkers to further improve clinical output.

The use of CT density as a possible surrogate parameter for malignant LN infiltration was discussed in a study on patients with breast cancer (*29*). In that trial, x-ray phase-contrast microtomography was used to assess the CT density of locoregional axillary LNs and was found to have a high potential for noninvasive LN staging. The use of surrogate metric parameters has also been demonstrated for malignant lymphomas. In a retrospective study, volumetric LN analysis significantly improved lesion classification over the commonly used long-axis diameter (*30*).

The potential for functional PET parameters that can serve as surrogate parameters for TNM staging in oncologic imaging has been demonstrated in a variety of published data. According to Cerfolio et al. (*31*), in ^{18}F-FDG PET/CT of LC patients, the SUV_{max} of the primary tumor is higher in higher-stage LC than in lower-stage LC. Cuaron et al., also studying LC patients, found that ^{18}F-FDG uptake by the primary tumor varies among tumor types (*32*), and Brown et al. found that this variation might be due to differences in the expression of glucose transporters (*33*).

Because of the uncertainties in noninvasive PET/CT-based oncologic imaging, it is often mandatory to use invasive staging techniques—such as core-cut biopsy of the primary tumor, possible LN metastases, or distant metastases—in clinical routine. In these cases, additional information from CT density–based semiautomated LN analysis, especially when combined with functional PET parameters such as SUV_{max}, may lead to high-yield targets for invasive staging. Because of the better prognostic predictability of TNM stages in noninvasive PET/CT imaging, the use of additional surrogate parameters such as CT density–based cutoffs for LN analyses may, over the long term, not only help locate high-yield targets for biopsy but also reduce the need for invasive staging procedures. As part of the recently evolving field of radiomics, it may be possible in future clinical routine to automatically generate CT density–based cutoffs as possible imaging biomarkers, thus helping to further categorize unclear imaging findings (*8*).

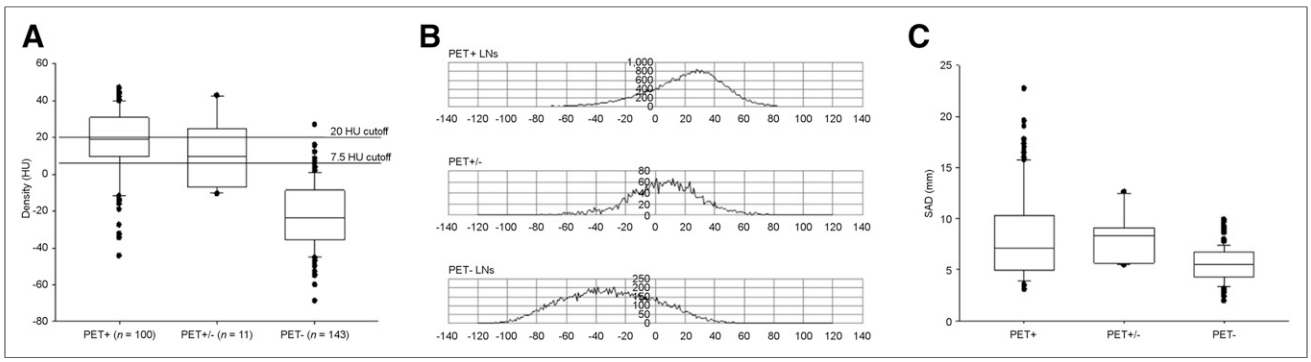

FIGURE 5. Statistical analysis of CT density in PCA patients. (A) Box plots with median and 95% confidence interval for PET+, PET+/−, and PET− LNs. (B) Averaged histograms for PET+, PET+/−, and PET− LNs. (C) Box plots with median, 25%, and 75% quartiles for PET+, PET+/−, and PET− LNs. *P* values for statistical analysis among subgroups are presented in Table 1.

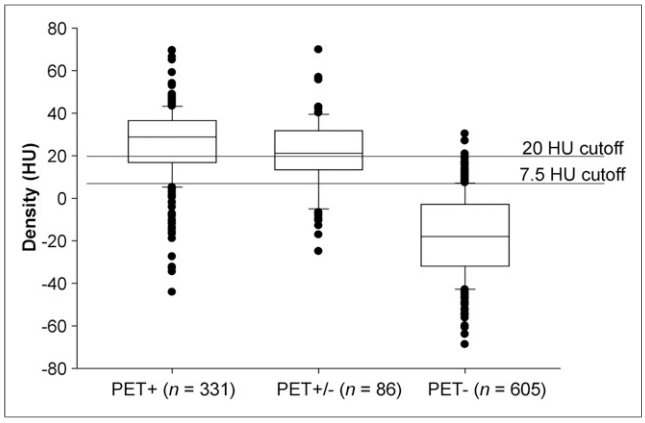

FIGURE 6. CT density: box plots with median, 25%, and 75% quartiles of PET+, PET+/−, and PET− LNs in patients irrespective of tumor type.

Some limitations of this study include its retrospective design and lack of histopathologic correlation for the PET and CT findings. To clearly define dedicated CT density–based cutoffs that can distinguish between malignant and benign LNs, it might be helpful to perform prospective studies for each of the tumor types discussed in this article, focusing on correlating preoperative PET/CT findings with histopathologic findings. However, restricting such studies to preoperative patients would lead to a focus on lower-stage cancer.

CONCLUSION

Semiautomated analysis of CT density in the LNs of patients with LC, MM, GEP NET, and PCA might become a valuable surrogate parameter to improve LN staging with PET/CT, using possible cutoffs of 7.5 HU to discriminate malignant from benign LNs and 20 HU to exclude LN benignancy.

DISCLOSURE

No potential conflict of interest relevant to this article was reported.

REFERENCES

1. Petersen H, Holdgaard PC, Madsen PH, et al. FDG PET/CT in cancer: comparison of actual use with literature-based recommendations. *Eur J Nucl Med Mol Imaging.* 2016;43:695–706.
2. Kratochwil C, Haberkorn U, Giesel FL. PET/CT for diagnostics and therapy stratification of lung cancer [in German]. *Radiologe.* 2010;50:684–691.
3. Pfluger T, Melzer HI, Schneider V, et al. PET/CT in malignant melanoma: contrast-enhanced CT versus plain low-dose CT. *Eur J Nucl Med Mol Imaging.* 2011;38:822–831.
4. Pfister D, Porres D, Heidenreich A, et al. Detection of recurrent prostate cancer lesions before salvage lymphadenectomy is more accurate with ^{68}Ga-PSMA-HBED-CC than with ^{18}F-fluoroethylcholine PET/CT. *Eur J Nucl Med Mol Imaging.* 2016;43:1410–1417.
5. Maxwell JE, Howe JR. Imaging in neuroendocrine tumors: an update for the clinician. *Int J Endocr Oncol.* 2015;2:159–168.
6. Flechsig P, Kratochwil C, Schwartz LH, et al. Quantitative volumetric CT-histogram analysis in N-staging of ^{18}F-FDG-equivocal patients with lung cancer. *J Nucl Med.* 2014;55:559–564.
7. Goeckenjan G, Sitter H, Thomas M, et al. Prevention, diagnosis, therapy, and follow-up of lung cancer: interdisciplinary guideline of the German Respiratory Society and the German Cancer Society—abridged version [in German]. *Pneumologie.* 2011;65:e51–e75.
8. Lambin P, Rios-Velazquez E, Leijenaar R, et al. Radiomics: extracting more information from medical images using advanced feature analysis. *Eur J Cancer.* 2012;48:441–446.
9. Shao T, Yu L, Li Y, Chen M. Density and SUV ratios from PET/CT in the detection of mediastinal lymph node metastasis in non-small cell lung cancer [in Chinese]. *Zhongguo Fei Ai Za Zhi.* 2015;18:155–160.
10. Flechsig P, Zechmann CM, Schreiweis J, et al. Qualitative and quantitative image analysis of CT and MR imaging in patients with neuroendocrine liver metastases in comparison to ^{68}Ga-DOTATOC PET. *Eur J Radiol.* 2015;84:1593–1600.
11. Giesel FL, Kratochwil C, Mehndiratta A, et al. Comparison of neuroendocrine tumor detection and characterization using DOTATOC-PET in correlation with contrast enhanced CT and delayed contrast enhanced MRI. *Eur J Radiol.* 2012;81:2820–2825.
12. Moltz JH, Bornemann L, Kuhnigk J-M, et al. Advanced segmentation techniques for lung nodules, liver metastases, and enlarged lymph nodes in CT scans. *IEEE J Sel Top Signal Process.* 2009;3:122–134.
13. Hellwig D, Graeter TP, Ukena D, et al. ^{18}F-FDG PET for mediastinal staging of lung cancer: which SUV threshold makes sense? *J Nucl Med.* 2007;48:1761–1766.
14. Danielsen M, Hojgaard L, Kjaer A, Fischer BM. Positron emission tomography in the follow-up of cutaneous malignant melanoma patients: a systematic review. *Am J Nucl Med Mol Imaging.* 2013;4:17–28.
15. Kwekkeboom DJ, Kam BL, van Essen M, et al. Somatostatin-receptor-based imaging and therapy of gastroenteropancreatic neuroendocrine tumors. *Endocr Relat Cancer.* 2010;17:R53–R73.
16. Flechsig P, Choyke P, Kratochwil C, et al. Increased x-ray attenuation in malignant vs. benign mediastinal nodes in an orthotopic model of lung cancer. *Diagn Interv Radiol.* 2016;22:35–39.
17. Toloza EM, Harpole L, McCrory DC. Noninvasive staging of non-small cell lung cancer: a review of the current evidence. *Chest.* 2003;123(suppl):137S–146S.
18. Birim O, Kappetein AP, Stijnen T, Bogers AJ. Meta-analysis of positron emission tomographic and computed tomographic imaging in detecting mediastinal lymph node metastases in nonsmall cell lung cancer. *Ann Thorac Surg.* 2005;79:375–382.
19. Schaefer NG, Hany TF, Taverna C, et al. Non-Hodgkin lymphoma and Hodgkin disease: coregistered FDG PET and CT at staging and restaging—do we need contrast-enhanced CT? *Radiology.* 2004;232:823–829.
20. Gould MK, Kuschner WG, Rydzak CE, et al. Test performance of positron emission tomography and computed tomography for mediastinal staging in patients with non-small-cell lung cancer: a meta-analysis. *Ann Intern Med.* 2003;139:879–892.
21. Silvestri GA, Gould MK, Margolis ML, et al. Noninvasive staging of non-small cell lung cancer: ACCP evidenced-based clinical practice guidelines (2nd edition). *Chest.* 2007;132(suppl):178S–201S.
22. Beyer F, Buerke B, Gerss J, et al. Prediction of lymph node metastases in NSCLC: three dimensional anatomical parameters do not substitute FDG-PET-CT. *Nuklearmedizin.* 2010;49:41–48.
23. Tournoy KG, Maddens S, Gosselin R, Van Maele G, van Meerbeeck JP, Kelles A. Integrated FDG-PET/CT does not make invasive staging of the intrathoracic lymph nodes in non-small cell lung cancer redundant: a prospective study. *Thorax.* 2007;62:696–701.
24. Miller AB, Hoogstraten B, Staquet M, Winkler A. Reporting results of cancer treatment. *Cancer.* 1981;47:207–214.
25. Therasse P, Arbuck SG, Eisenhauer EA, et al. New guidelines to evaluate the response to treatment in solid tumors. European Organization for Research and Treatment of Cancer, National Cancer Institute of the United States, National Cancer Institute of Canada. *J Natl Cancer Inst.* 2000;92:205–216.
26. Eisenhauer EA, Therasse P, Bogaerts J, et al. New response evaluation criteria in solid tumours: revised RECIST guideline (version 1.1). *Eur J Cancer.* 2009;45:228–247.
27. McIvor J, Siew T, Campbell A, McCarthy M. FDG PET in early stage cutaneous malignant melanoma. *J Med Imaging Radiat Oncol.* 2014;58:149–154.
28. Zattoni F, Guttilla A, Evangelista L. Can GA-PSMA or radiolabeled choline PET/CT guide salvage lymph node dissection in recurrent prostate cancer? *Eur J Nucl Med Mol Imaging.* 2016;43:1407–1409.
29. Jensen TH, Bech M, Binderup T, et al. Imaging of metastatic lymph nodes by x-ray phase-contrast micro-tomography. *PLoS One.* 2013;8:e54047.
30. Puesken M, Buerke B, Gerss J, et al. Prediction of lymph node manifestations in malignant lymphoma: significant role of volumetric compared with established metric lymph node analysis in multislice computed tomography. *J Comput Assist Tomogr.* 2010;34:564–569.
31. Cerfolio RJ, Bryant AS, Ohja B, Bartolucci AA. The maximum standardized uptake values on positron emission tomography of a non-small cell lung cancer predict stage, recurrence, and survival. *J Thorac Cardiovasc Surg.* 2005;130:151–159.
32. Cuaron J, Dunphy M, Rimner A. Role of FDG-PET scans in staging, response assessment, and follow-up care for non-small cell lung cancer. *Front Oncol.* 2013;2:208.
33. Brown RS, Leung JY, Kison PV, Zasadny KR, Flint A, Wahl RL. Glucose transporters and FDG uptake in untreated primary human non-small cell lung cancer. *J Nucl Med.* 1999;40:556–565.